ASSOCIATIE EURATOM-FOM

FOM-INSTITUUT VOOR PLASMAFYSICA

RIJNHUIZEN — NIEUWEGEIN — NEDERLAND

March 1986

OPTIMALIZATION STUDY FOR ION-TEMPERATURE MEASUREMENTS BY MEANS OF RUTHERFORD SCATTERING

by

A.J.H. Donné and E.P. Barbian

Rijnhuizen Report 86-164

This work was performed as part of the research programme of the association agreement of Euratom and the 'Stichting voor Fundamenteel Onderzoek der Materie' (FOM) with financial support from the 'Nederlandse Organisatie voor Zuiver-Wetenschappelijk Onderzoek' (ZWO) and Euratom.

OPTIMALIZATION STUDY FOR ION-TEMPERATURE MEASUREMENTS BY MEANS OF RUTHERFORD SCATTERING

by

A.J.H. Donné and E.P. Barbian
Association Euratom-FOM
FOM-Instituut voor Plasmafysica
Rijnhuizen, Nieuwegein, The Netherlands

ABSTRACT

Small-angle Rutherford scattering of energetic neutrals by plasma ions is governed by energy and momentum conservation. The FWHM of the scattering distribution reveals the ion temperature of the plasma. A feasibility study is performed to optimize the parameters in case Rutherford-scattering technique is applied to a medium-sized tokamak experiment.

Together with a time-of-flight analyser with a high energy resolution of about 100, a 20 keV helium probing beam with a neutral current density of 10 A/m^2 can provide a detailed spectrum within 3 ms, from which the ion temperature can be extracted with an accuracy of better than 10%. The influence of plasma impurities and resonant charge exchange on the scattering process is discussed in detail. The good spatial resolution makes the method very suitable to investigate energy deposition profiles in the case of ion-cyclotron radiation applied to the plasma for the purpose of plasma heating.

1. INTRODUCTION

The ion temperature of a hot plasma can be determined by a number of techniques, but as a general rule a good spatial resolution is not easily achieved. The most prominent method up-to-now to measure this important parameter is based on the analysis of charge-exchange neutrals which are created by ion-electron recombination or charge exchange with background neutrals, possibly additionally enhanced by beam-injected neutrals [1]. These charge-exchange neutrals can escape from the magnetically confined plasma and reflect the energy distribution of the plasma ions. An unpleasant circumstance, however, is the fact that the charge-exchange neutrals lose their local information when the plasma dimensions are large compared with the mean free path for re-ionization. At large plasmas like JET, TFTR or JT60 the very strong attenuation of charge-exchange neutrals makes the deduction of the central ion temperature virtually impossible.

A determination of the ion temperature through a measurement of the energy spectrum of thermonuclear neutrons is confused by several processes like the production of neutrons by reactions other than D-T or D-D [2].

Some space-resolving techniques were developed to measure the ion temperature in a plasma. For instance, the measurement of the Doppler broadening of spectral lines from high-Z impurities yields the local ion temperature [3]. This technique, however, becomes more difficult to apply as one succeeds in reducing the amount of high-Z components, for instance by carbonization of the limiters and the chamber walls.

There have also been efforts aimed at the determination of fusion plasma ion temperatures by means of collective Thomson scattering from thermal fluctuations [4]. The accuracy of this method is questionable due to the fact that the scattering form factors depend upon the electron temperature and upon the effective impurity concentration. Furthermore, the existence of non-thermal fluctuations can mask or disturb the ion feature. To date, there has not yet been a definitive thermal-scattering determination of the ion temperature in a plasma.

Recently, a proof-of-principle has been given to demonstrate that the ion temperature can be determined via cw far-infrared laser scattering from externally excited ion-Bernstein waves [5]. It is claimed that this method can yield the ion temperature with good accuracy and with a reasonable degree of localization. Problems arise from the fact that the measurement of the temperature is indirect, however, since one has to go through a great deal of interpretation to obtain the final result.

With the above diagnostic techniques it becomes even more difficult to identify contributions caused by deviations from a standard maxwellian velocity distribution, which can be expected during fast changes of the plasma profile, especially when additional heating techniques are applied.

A fundamentally more promising diagnostic technique makes use of the small-angle Rutherford scattering of energetic neutrals by the plasma ions. Energy and momentum conservation determine the spectrum of the elastically scattered neutrals, which apparently lose some energy on the average, and more relevant to the observation, experience a considerable broadening of the energy distribution due to the random motion of the encountered ions. The observational line intersects the probing beam under a small properly chosen angle to attain both a sufficient spatial resolution and a large enough flux of scattered particles for recording the spectrum.

The theory of small-angle Rutherford scattering is well-established; its application to plasma diagnostics was first proposed by V.G. Abramov et al. [6]. First measurements on a 0.5 keV plasma were carried out in 1978 at the T-4 tokamak by a group from the Ioffe Institute [7,8] with an 8 keV He-beam of 10 A/m^2. Further application of the neutral-beam scattering technique was proposed by H.J.B.M. Brocken et al. [9] and G. Notermans et al. [10]. A high-resolution time-of-flight analyser for detection of Rutherford-scattered neutrals was developed at Rijnhuizen. This analyser is designed to work in the highly radiative background near experimental fusion devices by applying a triple-coincidence detection method [11]. A prototype of the analyser was successfully used for the measurement of slowing-down spectra of neutral heating beams in ASDEX in 1984 [12,13].

Due to the large background of double charge-exchange neutrals, however, it became evident that an independent vertical probing beam has to be substantially a part of the Rutherford-scattering diagnostic. The choice of the beam species, the beam parameters and the scattering angle in relation with the expected plasma parameters is critical for the intended measurements. The aim of this work is to find proper conditions for a Rutherford-scattering diagnostic to be applied at a moderate large tokamak experiment. The optimalization calculations are performed on the basis of the TEXTOR parameters [14] and the properties of the time-of-flight analyser at hand.

In the following chapters, a short review of the applied formulae of the Rutherford-scattering theory is presented together with the line of

approach used for the optimalization procedure. Calculations considering the attenuation of the probing beam and the influence of the resonant charge-exchange process at the instant of the scattering are discussed in Chapter 3. Results are presented for the case of an ideal analyser neglecting instrumental effects in Chapter 4. From these data the proper parameters of the diagnostic array can be chosen.

The instrumental broadening of the TOF analyser is discussed in Chapter 5. On the basis of the chosen parameters, special attention is given to the possible influence of a typical plasma contamination with impurities like C and O, and moreover to the specific situation of a two-component plasma as used for the minority heating technique by means of ion-cyclotron radiation.

2. RUTHERFORD-SCATTERING THEORY

The change in momentum of an incident particle, scattered by a moving target particle, depends on the scattering angle, on the mass ratio of the two particles, and on their relative speeds. Hence, when scattering angle, mass ratio and beam momentum are fixed, the scattering will depend on the velocity of the target particle only. Accordingly, when a beam of mono-energetic particles passes through a plasma, the energy distribution of particles scattered within a fixed solid angle reflects the velocity distribution of the plasma ions. The temperature of the ions can be deduced from the latter distribution. The formulae describing the scattering process can be found in literature [6]. We shall only give a brief summary of the main results.

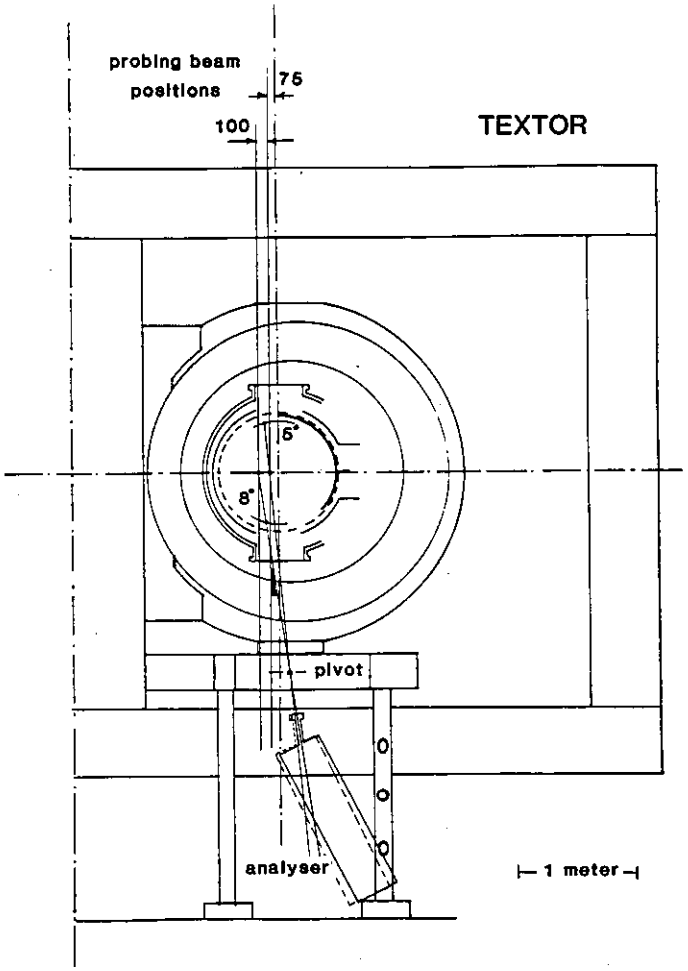

Fig. 1. Schematic representation of the proposed scattering experiment at TEXTOR.

The neutral counting rate at the position of the detector (see Fig. 1 for a schematic representation of the neutral-particle analyser proposed to be installed on TEXTOR) is given by:

$$d\Gamma = C(E)\eta(E)\,\frac{Jn_p}{2e}\,V_{scat}\,\frac{d\sigma}{d\Omega}\,\frac{dE}{E}\,d\Omega\ , \qquad (1)$$

with $C(E)$ a factor which takes into account the partial ionization of the neutral beam during the scattering process [13] (see Section 3.2);

$\eta(E)$ the energy-dependent attenuation of the beam in the plasma (see Section 3.1);

n_p the local ion density in the plasma (m^{-3});

J/e the neutral-beam intensity ($m^{-2}\ s^{-1}$);

V_{scat} the scattering volume (m^3);

E the energy of a detected neutral particle (eV);

$d\Omega$ the solid angle of acceptance.

The differential scattering cross-section $d\sigma/d\Omega$ is given by

$$\frac{d\sigma}{d\Omega} = \sqrt{\frac{4}{\gamma\pi E_d E_b T}}\,E^{3/2}\,\left\{\frac{Z_p Z_b e}{4\pi\varepsilon_o E_d}\right\}^2\,\exp\left\{\frac{-[E-(E_b-\gamma E_d)]^2}{4\gamma E_d T}\right\}\ , \qquad (2)$$

in which

γ is the mass ratio of beam and plasma particle = m_b/m_p;

E_b is the beam energy of the neutrals (eV);

T is the local ion temperature in the scattering volume (eV);

Z_b, Z_p are the nuclear-charge numbers of the beam and plasma particle, respectively,

and

$$E_d \equiv E_b + E - 2\sqrt{E\cdot E_b}\,\cos\,\theta\ .$$

It can be shown that

$$E_d \simeq E_b \sin^2\theta \quad \text{for } E_b \gg T\ . \qquad (3)$$

The scattering volume is defined by the intersection of the beam with the line of sight of the analyser (see Fig. 2),

$$V_{scat} = \frac{\pi h^2}{4} \frac{2R_b}{\sin\theta} = \frac{\pi h^2}{4} \Delta x_s \ , \qquad (4)$$

with h the diameter of the line of sight;
R_b the radius of the neutral beam;
θ the scattering angle;
and Δx_s the length of the scattering volume ($\equiv 2R_b/\sin\theta$).

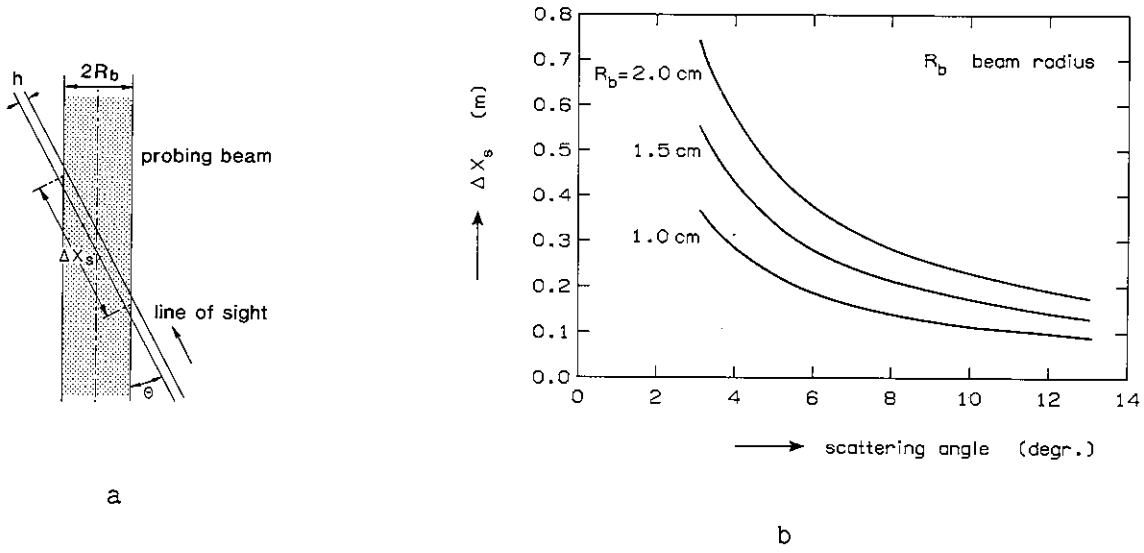

Fig. 2. a. Schematic representation of the scattering volume.
b. Dependence of the length of the scattering volume on the beam radius and on the scattering angle.

The full width at half maximum (FWHM) of the distribution for $E_b >> T$ and for small scattering angles, is determined by the local ion temperature,

$$\Delta E_{1/2} \approx 4 \sin\theta \sqrt{\gamma E_b T \ell n 2} \ . \qquad (5)$$

The maximum of the distribution is found at

$$E_o \approx E_b \left[\frac{\gamma \cos\theta + \sqrt{1-\gamma^2 \sin^2\theta}}{1+\gamma} \right]^2 . \qquad (6)$$

With Eqs. (1)-(6) one is able to calculate the energy distribution of the scattered neutrals if the temperature is known (for instance, in the optimalization calculations to be presented below). In an actual experiment, the temperature can be deduced from the scattering distribution by means of Eq. (5).

3. CALCULATION OF THE DISTRIBUTION IN AN IDEAL ANALYSER

In designing diagnostic instrumentation based on single Rutherford scattering, the following factors should be taken into account:

1. The choice of the mass of the probing particles, m_b, is important, as was already discussed by Berezovskii et al. [8]. The attenuation of the beam in the plasma, and the resonant charge-exchange processes are strongly dependent on m_b (see Section 2.1 and 2.2). Furthermore, for a given ion source the maximum current density decreases with increasing particle mass.
2. The choice of the beam energy is of further importance. According to Eqs. (1)-(6), there is an explicit dependence of the scattering yield on E_b (roughly as $E_b^{-5/2}$). There also exists an implicit dependence due to the attenuation and the resonant charge exchange, which are both strongly dependent on the energy (see Sections 2.1 and 2.2).
3. The scattering angle θ should be chosen on the one hand as large as possible in order to get a good spatial resolution. On the other hand, the yield decreases sharply as a function of scattering angle, so that a compromise will have to be found between the scattering yield and the spatial resolution. Some more, but less stringent boundary conditions arise at very small scattering angles, when one has to keep away from the cone of primary or multiple-scattered neutrals or at very large scattering angles where the scattering distribution might become broader than the chosen finite bandwidth of the apparatus.

Following a number of considerations, a recommendation can be given for the optimal configuration to perform a Rutherford-scattering experiment at TEXTOR. Since m_b must preferentially be taken small [8], we shall only consider H and He as the most promising choices for beam species.

3.1 Attenuation of the probing beam in the plasma

The attenuation of the beam in the plasma can be described by

$$\eta(E) = \exp\{-\int dx/\lambda(x)\} \approx \exp\{-\ell/\lambda(E)\} \ , \qquad (7)$$

with ℓ the total path length in the plasma and $\lambda(E)$ the mean free path for ionization and charge exchange of the neutral beam, which can be written as:

$$\lambda(E) = \left\{ n_p \left(\sigma_{cx}(E) + \sigma_{ion}(E) \right) + n_e \frac{\langle \sigma_e v \rangle}{v_o} + n_{beam} \sigma_{cx}(\Delta E) \right\} , \qquad (8)$$

with n_p, n_e, n_{beam} the local ion, electron and neutral density in the scattering volume, respectively;

$\sigma_{cx}, \sigma_{ion}$ the cross-section for charge exchange and ionization by protons, respectively;

$\langle \sigma_e v \rangle$ the rate coefficient for ionization by electrons;

v_o the velocity of the neutral particle.

The third term in Eq. (8) is due to charge exchange between two neutral probing particles in the beam, which have different energies, ΔE, with respect to each other due to the voltage ripple in the ion source. For high beam energies (> 5 keV) this term is negligible compared with the others. The contribution from ionization by electrons is smaller than the first contribution in case of a hydrogen beam. For He probing particles, however, it dominates the cross-section at low energies.

The charge-exchange and ionization cross-sections have been extensively measured. Freeman and Jones [15,16] combined all experimental information and parametrized the cross-sections as

$$\sigma = \exp\left\{ \sum_{i=0}^{n} A_i (\ell n E)^i \right\} .$$

The parameters, necessary to calculate the relevant cross-sections in case that a H- or a He-neutral beam is used, are listed in Table 1.

TABLE 1

Parametrization of the charge-exchange and ionization cross-sections			
	Ionization		Charge exchange*
	$H^0+p \rightarrow p+p+e^-$	$He^0+p \rightarrow He^+ +p+e^-$	$He^0+p \rightarrow He^+ +H^0$
A_0	-0.4203309×10^{2}	-0.4075642×10^{2}	-0.4040162×10^{2}
A_1	0.3557321×10^{1}	0.1556363×10^{1}	0.2307004×10^{1}
A_2	-0.1045134×10^{1}	-0.8902739	-0.1713230×10^{1}
A_3	0.3139238	0.5443478	0.1351025×10^{1}
A_4	-0.7454475×10^{-1}	-0.1435067	-0.4566584
A_5	0.8459113×10^{-2}	0.1590320×10^{-1}	0.6353690×10^{-1}
A_6	-0.3495444×10^{-3}	-0.6330861×10^{-3}	-0.3139240×10^{-2}

* The charge-exchange process $H^0+p \rightarrow p+H^0$ is parametrized as

$$\sigma = \frac{0.6937\times10^{-14}(1-0.155 \log E)^2}{1+0.1112\times10^{-14}\ E^{3.3}}$$

3.2 Resonant charge exchange

When an atom is scattered by an ion, there is a finite chance that the atom exchanges an electron with the ion. The probability for electron loss as a function of incident atom energy shows a number of pronounced peaks [8,17,18]. The resonance process might be explained qualitatively as follows. When the collision time is equal to an integer number times the revolution time of the electron around the atom, the interaction time between ion and electron is maximal, and the probability function for electron loss shows a resonance.

Accurate measurements on resonant electron loss in hydrogen-proton and helium-proton collisions were performed by Ziemba and Lockwood [17,18]. These measurements can be explained by a simple empirical relation

$$C(E) = 1 - k_1(E) - k_2(E)\sin^2[\alpha/\sqrt{E}-\beta\pi] \ , \qquad (9)$$

with

$$k_1(E) = a_1E^{-1}+a_2+a_3E+a_4E^2 \ ,$$
$$k_2(E) = b_1E^{-1}+b_2+b_3E \ .$$

Besides measurements with protons as target atoms, Ziemba and Lockwood also parametrized the resonant electron loss in helium-helium collisions. The functions $k_1(E)$ and $k_2(E)$ are then parametrized as

$$k_1(E) = a_1/\ln(E) + a_2\exp\left(-a_3(E-a_4)^2\right) \text{ and}$$
$$k_2(E) = b_1-b_2\exp(-b_3\cdot E^2) \ .$$

The parameters α, β, a_i and b_i for hydrogen-proton, helium-proton and helium-helium scattering are given in Table 2.

TABLE 2

Parameters to describe the resonant charge-exchange process

	H + p	He + p	He+He
α	349.6	464.3	1115.5
β	0.28	0.26	0.23
a_1	-100.5	0	2.7
a_2	0.775	0	-0.086
a_3	0	2.5×10^{-5}	8.0×10^{-8}
a_4	0	3.0×10^{-10}	1.35×10^{4}
b_1	244.2	0	0.38
b_2	0.10	0.02	0.175
b_3	0	1.5×10^{-7}	1.7×10^{-8}

The probability for resonant charge exchange is independent of the scattering angle in the angle range of the proposed experiment (5-10°).

For scattering of hydrogen and helium on heavy impurities like C, O, and Fe, however, very scarce experimental information on electron-loss processes is available. A general feature is that for scattering on heavy ions the probability for electron loss is a smooth function of the probing-beam energy [18]. Takeuchi et al. [19] measured a difference between Rutherford-scattering theory and experiment for scattering of protons from He, Ne and Ar. Earlier, E. Berezovskii et al. [8] experienced at T-4 that elastic scattering on even a few percent of impurities can be considered negligible compared to that of the protons, in spite of the fact that a comparable contribution had to be expected from the Z^2 dependence in Eq. (2). Aware of the fact that the contribution of impurities to the scattering distribution needs further investigation, we apply the 95% probability for electron loss as determined by Takeuchi et al. [19] in the case of scattering from heavy atoms like C, O and Fe.

3.3 Scattering yield in a realistic analyser

With the aid of Eqs. (1)-(9) it is possible to calculate the complete scattering distribution, first considering an ideal experiment, which means that the analyser is assumed to have no instrumental broadening and a detection efficiency of 100%. In case of a plasma with impurities added ($Z_{eff} > 1$), the total scattering distribution will be a sum of individual gaussian distributions arising from the different constituents of the plasma.

Although it is possible to calculate the complete scattering distribution directly, it is more convenient to calculate the yield at the top of the distribution (where the exponential term in Eq. (2) equals 1), the full width at half maximum and also the position of the maximum. The distribution may then be calculated from these three parameters.

From Eqs. (1)-(6) we can derive an expression for the yield at the top of the distribution

$$\Gamma_{top} = C(E)\eta(E)Jn_p\Delta x_s \frac{1}{E_b^3}\left(\frac{E}{T}\right)^{1/2} \frac{1}{\sin^5\theta} \frac{7.30Z_p^2Z_b^2}{\sqrt{\gamma}} \left[\frac{\gamma\cos\theta+\sqrt{1-\gamma^2\sin^2\theta}}{1+\gamma}\right] . \quad (10)$$

To obtain the yield which is measured by the analyser, Γ_{top} has to be multiplied by some experimental parameters:

$$\Gamma_a = \Gamma_{top} A d\Omega_a \xi \ , \tag{11}$$

with A the cross-section of the line of sight (m^2);

$d\Omega_a$ the solid angle of acceptance of the analyser (sr);

and ξ the detection efficiency of the analyser.

The total integrated flux in the distribution is given by

$$\Gamma_{total} = \Gamma_a \Delta E_{\frac{1}{2}} \ . \tag{12}$$

In case of a polluted plasma ($Z_{eff} > 1$) the scattering distribution can be calculated as being a sum of gaussian distributions arising from the individual impurities in the plasma.

Equations (5)-(6) and (10)-(12) are sufficient to calculate the distribution in case of an analyser which has a negligible instrumental broadening compared with the thermal broadening (Eq. (5)). Since the calculation of the instrumental width is not straightforward, we shall first present the "ideal" results in the succeeding chapter. Finally the formulae for calculation of instrumental effects and the results of such a calculation are presented in Chapter 5.

4. RESULTS FOR AN IDEAL ANALYSER

Equations (1)-(12) are embedded in a computer programme YIELD.PAS, which calculates the scattering yield for pure and impure plasmas. For the results to be presented in this and the succeeding chapter, we used TEXTOR parameters [14] for input (see Table 3). The central and mean ion densities were deduced from the density profile for a typical TEXTOR shot (nr. 15629) at t = 500 ms (see Fig. 3). The central ion temperature in the same shot was 800 eV.

TABLE 3

Input parameters for TEXTOR

Main radius R	1.75 m
Small radius a	0.45 m
Central ion temperature T	800.0-2000.0 eV
Central ion density	4.5×10^{19} m^{-3}
Mean ion density	2.9×10^{19} m^{-3}.

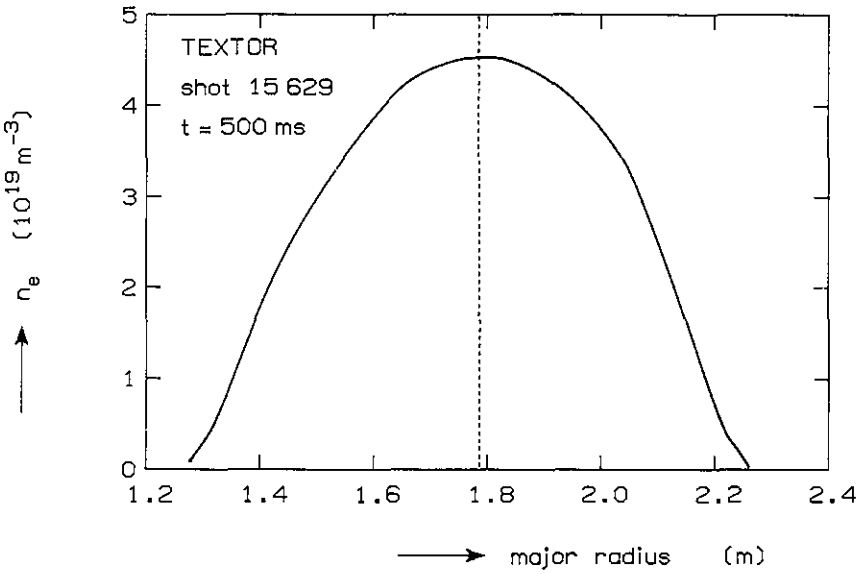

Fig. 3. Density profile for a typical TEXTOR shot at t = 500 ms.

For the parameters of the ion source, we took the values of the Bonnal source, presently used to produce a diagnostic beam in the TORTUR III tokamak at Rijnhuizen (see Table 4). Since the Bonnal ion source could have an improper energy range for the Rutherford-scattering experiment, we will

perform calculations at other energies as well. In Table 5, the parameters of the improved time-of-flight analyser, proposed to be installed at TEXTOR, are listed.

TABLE 4

Parameters of the Bonnal-ion source

Beam energy E_b	20-25 keV
Neutral-beam radius R_b	0.02 m
Current density j_b	10.0 A/m^2

TABLE 5

Parameters of the Rijnhuizen time-of-flight analyser

Detector sensitive area A	7×10^{-5} m^2
Detector solid angle $d\Omega_a$	4×10^{-5} sr
Detection efficiency	0.01

Besides calculations in which all input parameters were fixed (T = 800 eV, E_b = 20 keV and θ = 5°) calculations were performed in which one of the main parameters was varied within a range accessible to the experiment.

Firstly, the mean free path for the neutrals in the plasma was calculated from the parametrized cross-sections of Freeman and Jones [15,16]. The result is given in Fig. 4a for H, and Fig. 4b for He, respectively. The mean free path for H increases monotonically with beam energy, whereas that for He has a maximum around 20-30 keV. In this energy range, the mean free path for He is four times larger than that for H, which means that the attenuation of a He-beam is seven times smaller than that of a H-beam.

Secondly, the resonant scattering factor C(E) was calculated by means of Eq. (9) and the parameters from Table 2. The results are plotted in Figs. 5a and 5b for H and He, respectively. For both probing particles, the resonant scattering is a strongly varying function of energy, with several pronounced maxima and minima. For H (see Fig. 5a), the factor C(E) equals 0.1-0.2 in the energy region of interest (20-30 keV), whereas that for He is 0.85-0.95. Hence, the number of He-neutrals, which is ionized simultaneously with the scattering process is one order of magnitude smaller than the number of H-neutrals.

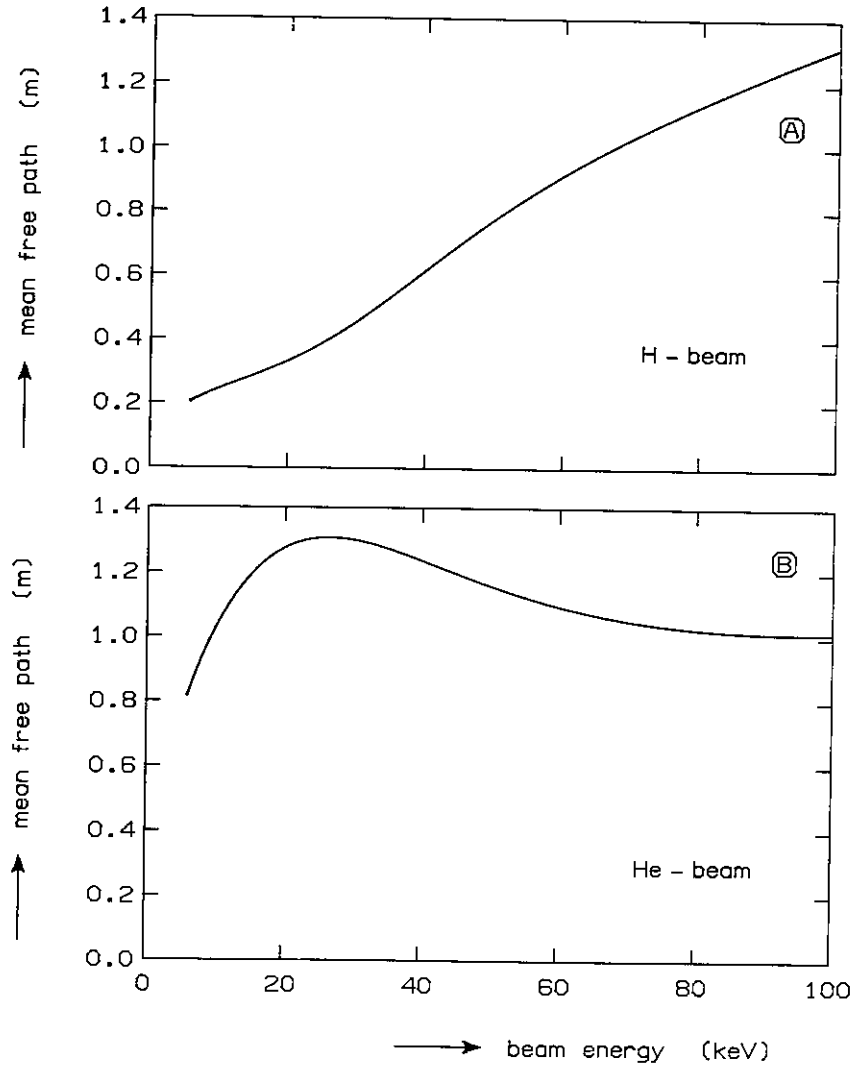

Fig. 4. Mean free path for charge exchange and ionization by protons and electrons for a H-beam (A) and a He-beam (B).

With this data, the distribution of scattered neutrals was calculated, using the standard input parameters (see Tables 3-5), taking also into account the data of the analyser. The results are listed in Tables 6 and 7 for H and He, respectively. It appears that the scattering yield at the top of the distribution for He is two orders of magnitude larger than that for H. Since the FWHM of the scattering distribution scales with $\sqrt{Y}$ (see Eq. (5)), the integrated flux for He is about a factor 200 larger than that for H. The significance of this result is that when using a He-probing beam it is possible to measure the local ion temperature in shorter time intervals than when using a H-beam. This is very advantageous in cases where one is interested in the time evolution of the ion temperature.

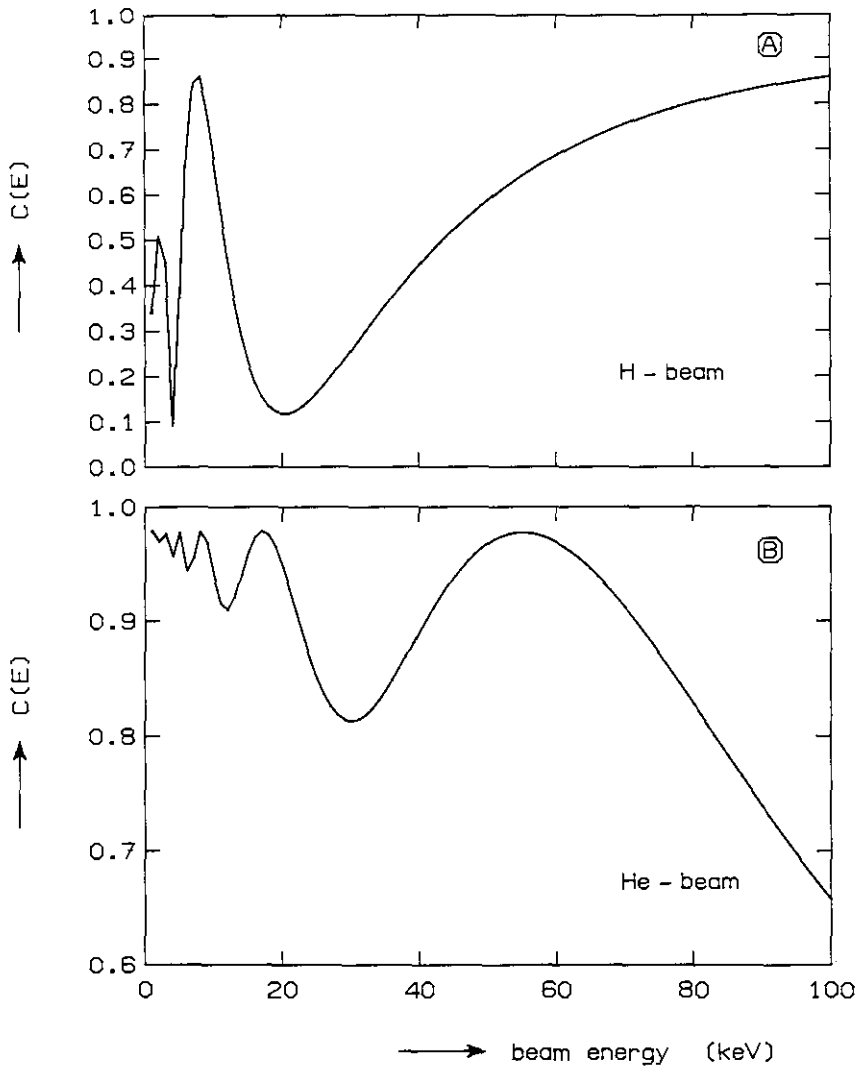

Fig. 5. Reduction factor due to resonant charge exchange for a H-beam (A) and a He-beam (B) in a hydrogen or deuterium plasma.

TABLE 6

Output parameters in case of a H-probing beam

Resonant charge-exchange factor C(E)	0.12
H - p charge-exchange cross-section	6.6×10^{-20} m^2
H - p ionization cross-section	1.4×10^{-20} m^2
H - e ionization cross-section	2.5×10^{-20} m^2
Mean free path λ	0.33 m
Attenuation	0.07
Length of scattering volume	0.46 m
Yield at top of distribution	1.4×10^{12} eV^{-1}s^{-1}m^{-2}sr^{-1}
Top yield in realistic analyser	42.3 eV^{-1} s^{-1}
FWHM of the scattering distribution	1161 eV
Integrated counting rate	4.9×10^{4} s^{-1}
Position of distribution maximum	19924 eV

TABLE 7

Output parameters in case of a He-probing beam

Resonant charge-exchange factor C(E)	0.95
He - p charge-exchange cross-section	3.4×10^{-21} m^2
He - p ionization cross-section	1.1×10^{-21} m^2
He - e ionization cross-section	2.3×10^{-20} m^2
Mean free path λ	1.27 m
Attenuation	0.49
Length of scattering volume	0.46 m
Yield at top of distribution	1.7×10^{14} eV^{-1} s^{-1}m^{-2}sr^{-1}
Top yield in realistic analyser	5008 eV^{-1} s^{-1}
FWHM of the scattering distribution	2322 eV
Integrated counting rate	1.2×10^{7} s^{-1}
Position of distribution maximum	19688 eV

One has to be aware of the fact that we used the same beam current for H and He. In reality, the H-beam current will be larger than the He-current, which one can obtain from the same source. This means that the top yield to be expected for H can be still somewhat larger than the value listed in Table 6.

The scattering yield was also calculated as a function of energy of the probing particles for selected values of the scattering angle θ. The results are plotted in Figs. 6a and 6b for H and He, respectively. There are two large differences between both figures. Firstly, the scattering yield for H varies strongly with energy, whereas that for He is rather smooth. Secondly, the absolute yield for He is about two orders of magnitude larger than that for H in the entire energy range. Around E_b = 20 keV there is a deep minimum in the curve for H, which would coincide with the working range of our ion source.

The dependence on the scattering angle is similar for both beam particles. The scattering yield decreases strongly with increasing scattering angle (see Figs. 7a and 7b). Hence, a small scattering angle is preferable on the one hand; on the other hand, the spatial resolution along the line of sight is inversely proportional to the scattering angle. An optimum has to be found on the basis of these considerations. In practice, one will choose the proper scattering angle to ensure the yield to be still large enough for accurate temperature measurements in short time intervals. An additional constraint is, in principle, that the scattering angle must be large enough to prevent non-scattered particles from entering the analyser.

The scattering angle should also be chosen small enough, so that the energy distribution falls completely within the bandwidth of the analyser.

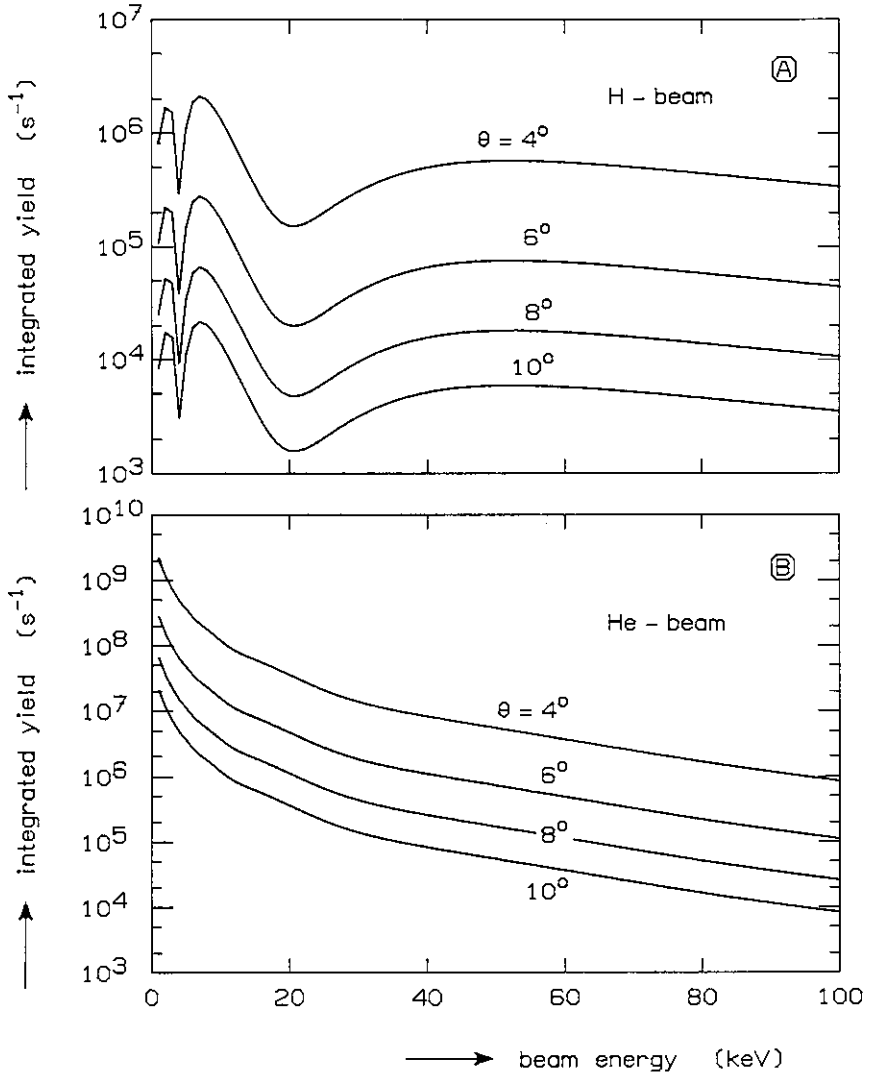

Fig. 6. Total integrated scattering yield as a function of beam energy E_b for some values of the scattering angle.
Fig. 6a: in case of a H-beam; Fig. 6b: in case of a He-beam.
The curves do not depend on the ion temperature.

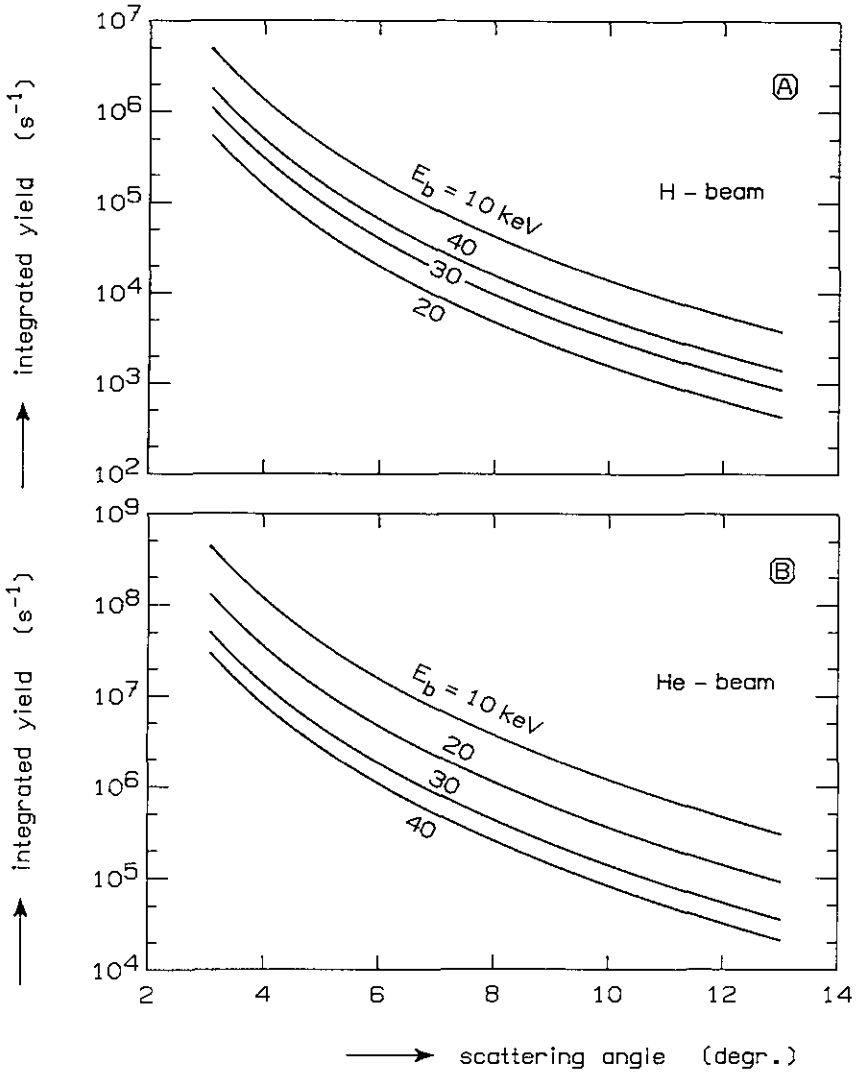

Fig. 7. Total integrated scattering yield as a function of scattering angle θ for several values of the beam energy of a H-beam (A) and a He-beam (B). The curves do not depend on the ion temperature.

Looking in a different way, we plotted the total expected scattering distributions for H and He, respectively, for some values of the scattering angle (Figs. 8a and 8b). Again, it is clear that the yield decreases sharply with increasing scattering angle, whereas the FWHM of the distribution increases more or less proportional to the scattering angle (see Eq. (5)).

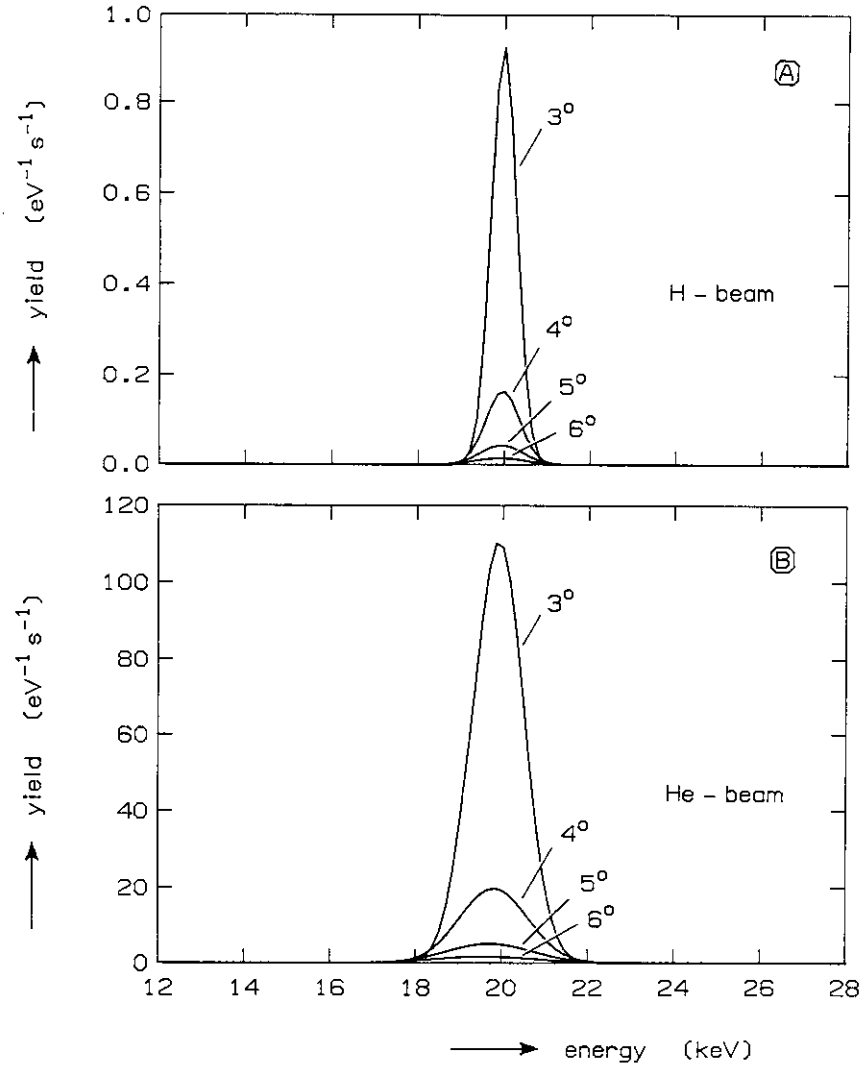

Fig. 8. Total scattering distribution for some values of the scattering angle θ for a H-beam (Fig. 8a) and a He-beam (Fig. 8b) in a 800 eV hydrogen plasma.

To get an idea how the width of the distribution scales as a function of temperature, we plotted the total distribution for several values of the temperature (see Figs. 9a and 9b for H and He, respectively). The FWHM increases distinctly with higher ion temperature. It was estimated by Notermans [10] that at least 200 counts are needed in one distribution to allow for a determination of the temperature to within 10% accuracy. For H as probing particle this means that the temperature could be determined within 4 ms and for He much faster. A minimum time is defined, however, by the finite accumulation time needed for one spectrum which is 1 ms, as determined by the dead time in the detector electronics. This time resolution is sufficiently small to measure the evolution of the local ion temperature concerning sawtooth-induced effects in tokamaks.

If one observes experimentally the thermal distribution, it becomes necessary to consider also the influence of the instrumental broadening, which is superimposed on the primary distribution as created by the scattering process. This subject will be discussed in the next chapter.

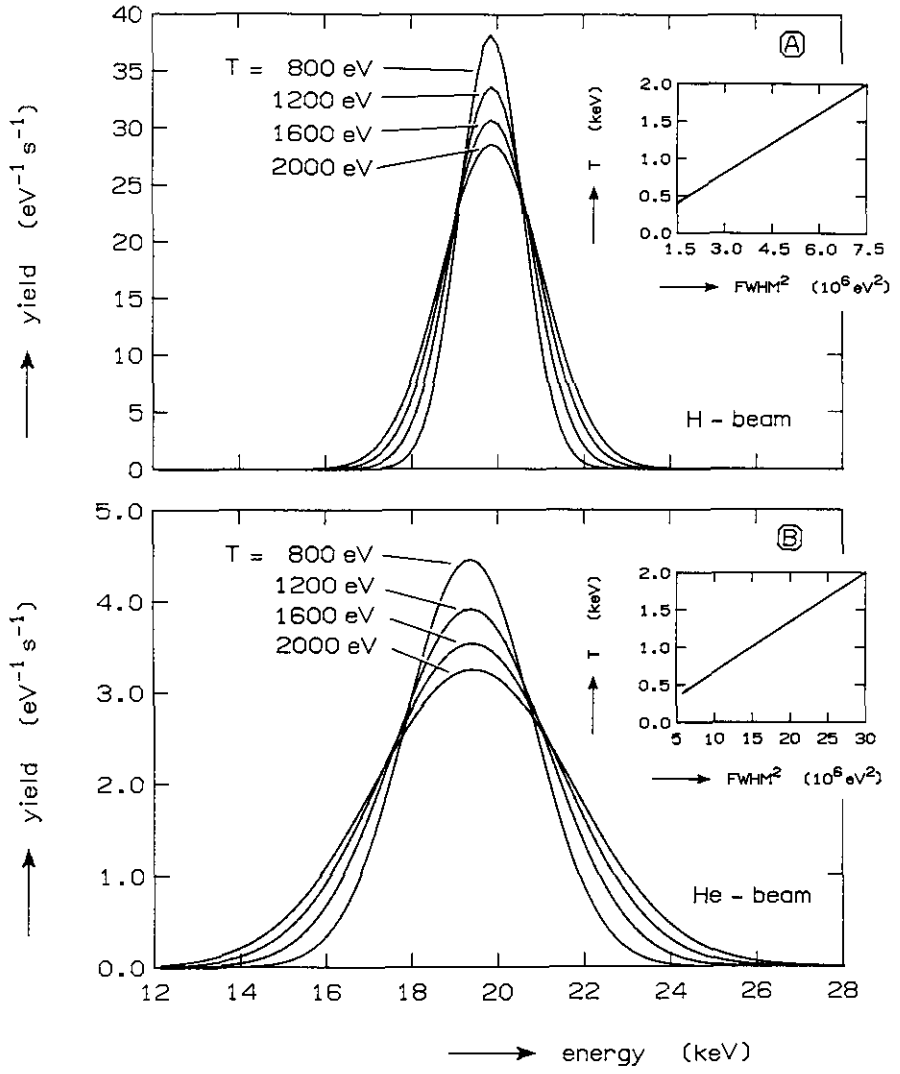

Fig. 9. Total scattering distribution for several values of the local ion temperature T for a H-beam (Fig. 9a) and a He-beam (Fig. 9b) at a scattering angle of 5°. The inset in both figures shows the dependence of T on the FWHM of the distribution.

5. INSTRUMENTAL BROADENING OF THE ANALYSER

A schematic representation of the analyser is given in Fig. 10. The time-of-flight (TOF) analyser consists of the following parts:

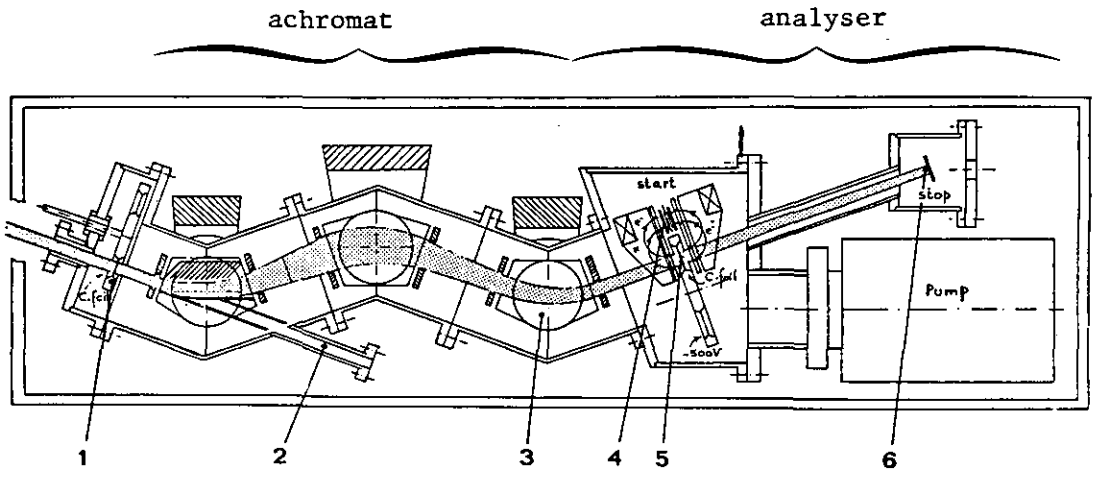

Fig. 10. Cross-sectional view of the TOF analyser:
1. ionizing carbon foil
2. viewing dump
3. sector magnet
4. start detector
5. start foil
6. stop detector.

1) A thin (- 5 μg cm^{-2}) carbon foil at the entrance to ionize the neutrals entering the chamber.
2) A preselecting achromat to separate the neutrals in the desired energy range from background particles and photons.
3) The TOF analyser itself, which measures the velocity of a particle by determining its flight time over a fixed distance. The instant at which the particle starts traversing the flight path is recorded by detecting the secondary electrons that are emitted when the particle traverses a second thin carbon foil. The particle itself produces the stop signal by hitting a detector at the end of the flight path. The secondary electrons are accelerated by means of an electric field and deflected over 180° by a small magnetic field before they are detected. Since secondary electrons are released both in forward and in backward direction from the foil, a coincident detection is possible by combining the signals from both start detectors with that from the stop detector. Such a triple-coincidence technique enables the use of the TOF detector in highly radiative enviroments.

The formulae for calculation of the instrumental width were extensively described by Notermans et al. [11]. Here we shall only give his final result for the spread in the measurement of the flight time of the neutrals (see Fig. 10):

$$(dt)^2 = \{(\frac{dx_o}{x_o})^2 + \frac{1}{4E^2}[(dV)^2 + \Omega^2 + (\frac{V_f}{2})^2]\} \frac{x_o^2}{2\frac{eE}{Mm}} + (dt_e)^2 , \qquad (13)$$

with

dt	the standard deviation in the measured flight time (s);
x_o,dx_o	the flight-path length (m) and its spread (m);
dV	the ripple in the acceleration voltage of the ion source (eV);
Ω	the energy straggling inside the start foil (eV);
V_f	the foil potential (eV) which equals the acceleration potential for secondary electrons;
E	the energy of the neutral particle (eV);
dt_e	the standard deviation in the flight time of the secondary electrons (s);
M	the mass number of the neutral particle;
e,m	the proton charge and rest mass, respectively.

The relative deviation in the flight-path length (dx_o/x_o) is caused by several effects, with the largest of these the angular spread of the neutral beam due to multiple scattering in the start foil. Furthermore, there is a contribution from the non-zero opening angle of the beam line and from wrinkles in the start foil.

The term $(dV)^2$ is due to the ripple in the acceleration voltage of the ion source. The straggling term Ω^2 is weakly dependent on the energy [20]. The term $(V_f/2)^2$ stems from partial neutralization of the particle beam by interactions in the foil.

The last term in Eq. (13) is arising from the deviation in the flight time of the secondary electrons, which is due to inhomogeneities of the magnetic field that deflects the electrons.

Equation (13) is incorporated in the computer programme YIELD.PAS. In Table 8, the input parameters for calculation of the instrumental broadening are listed. Moreover, the relative contributions to the instrumental broadening (see Eq. (13)) for H- and He-probing beams are given in the same table. The contributions are listed relative to each other, with the largest of them set to 1.0. The systematic error involving the instrumental broadening is not strongly dependent on the choice of probing particle. The

effect of the instrumental broadening on the total width of the distribution is shown in Figs. 11a and 11b for a H- and a He-beam scattering over 7.5° in a hydrogen plasma, respectively. In both figures, the scattering distribution is plotted with and without instrumental effects.

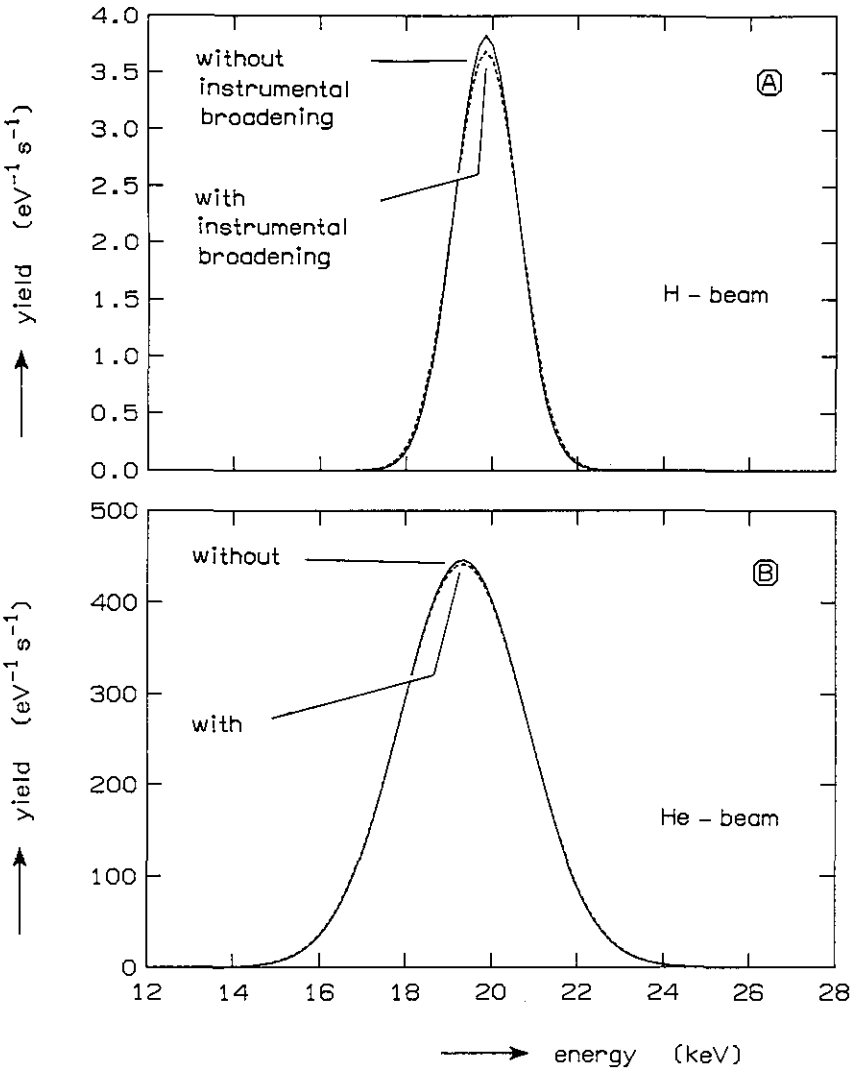

Fig. 11. Effect of the instrumental broadening upon the total distribution for scattering of H (Fig. 11a) and He (Fig. 11b) in a T = 800 eV hydrogen plasma.

For H, the instrumental effects enhance the thermal broadening by 8.4% (for $\theta = 5°$), for He only by 2.1%. This is due to the fact that the thermal width of the He distribution is 2 times larger than that for H.

It has to be emphasized that the different terms contributing to the instrumental broadening can be improved [11] such that the absolute instrumental width is about $\Delta E = 0.01\ E_b$.

In Fig. 12b, the instrumental distribution is presented, along with the total distribution at T = 800 eV for a He-beam in a hydrogen plasma. The instrumental broadening is equivalent to an ion temperature T = 20 eV.

The figure indicates that also structures on top of the distribution could be detected with the TOF analyser. This is especially valuable if one studies non-maxwellian plasmas.

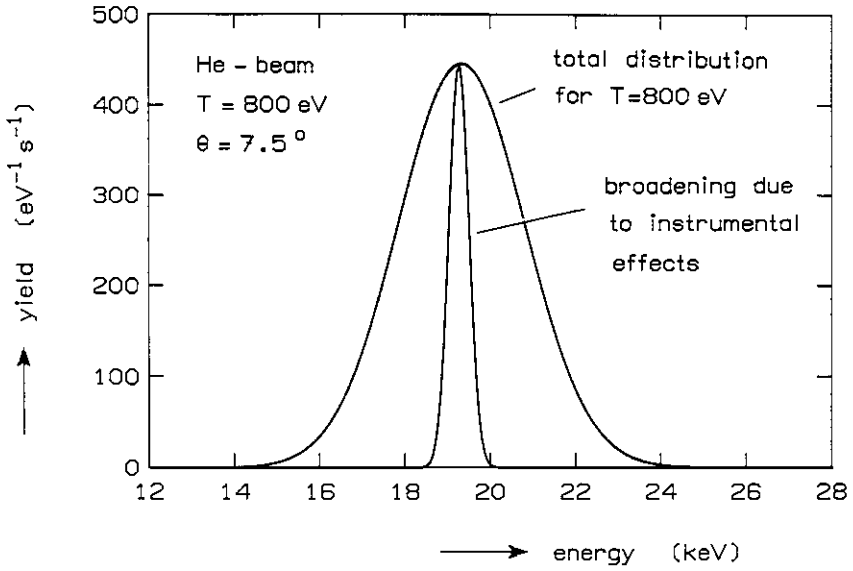

Fig. 12. Total distribution for scattering of a He-beam in a T = 800 eV hydrogen plasma along with the instrumental function.

TABLE 8

Instrumental effects

Radius of channelplate	9 mm
Distance start foil - stop detector	0.30 m
Wrinkles in the foil	1 mm
Fixed opening angle of the beam line	1.0°
Charge number of the foil particles	6
Foil surface density	5.0 μg cm^{-2}
Foil voltage	540 V
Ripple in source voltage	1.0%
Magnetic field secondary electrons	4 mT
Inhomogeneity of magnetic field	0.2 mT

Relative contributions (arbitrary units) to the instrumental width

Due to:	differences in the flight path length	0.2
	ripple in the source voltage	0.3
	energy straggling in the start foil	1.0
	partial neutralization in the start foil	0.5
	flight-time differences of secondary electrons	4×10^{-5}
Total instrumental width		488 eV
Total width of the distribution		1259 eV

TABLE 8 (continued)

Relative contributions (arbitrary units) to the instrumental width

Due to: differences in the flight path length	0.2
ripple in the source voltage	0.3
energy straggling in the start foil	1.0
partial neutralization in the start foil	0.7
flight-time differences of secondary electrons	1×10^{-5}
Total instrumental width	487 eV
Total width of the distribution	2373 eV

6. IMPURITIES

Up to now we did not investigate scattering by impurities in the plasma. A real plasma will contain impurities like oxygen, carbon and heavy elements as iron, nickel and chromium. To study the effects of these different elements, we compared their separately calculated contributions with the hydrogen (plasma) distribution.

Recently, carbonization of the walls is applied at TEXTOR, which leads to a decrease of metal impurities in the core. The total concentration of heavy metals is now less than 10^{-5} [21], the fraction of oxygen is less than 0.5%, whereas the carbon fraction in the core is 1-2.5%. For our calculations we took the following impurity concentrations: 2% C, 0.5% O and 0.001% Fe. The separate distributions were weighted with the corresponding abundances. For scattering of H- and He-particles from C, O and Fe we took $C(E) = 0.95$ (see Section 3.2); for scattering from H, D, and ^{3}He we used the parametrizations by Ziemba and Lockwood [17,18]. Scattering of H and He by the iron impurities in the plasma turned out to be negligible in all cases.

In Figs. 13a and 13b, the expected total scattering distributions are plotted for an impure plasma with the contributions of all components added up. The surface below each curve is proportional to the number of beam particles scattered from the corresponding impurities. In the calculation we have taken the instrumental broadening into account. For a hydrogen beam (Fig. 13a), it is clear that the peak arising from the protons in the plasma only makes up 50% of the total distribution. This means that H-probing beams can only be used for a determination of the ion temperature in a plasma when the impurity concentrations are well known. On the other hand, the complementary use of H may be very interesting for the sensitive deduction of impurity numbers.

Although it is also not possible to neglect the scattering from impurities in case that a He-beam is used, it can be stated that in this case the ion temperature is still measurable. This is partly due to the fact that the relative strength of the impurity distributions is smaller for He than for H. Furthermore, the asymmetry in the total distribution is very helpful in separating impurity contributions from those of protons. Preferentially at larger scattering angles, the impurities can be separated from the protons due to the different peak positions of the distributions. This is indicated in Fig. 14, where the total scattering distributions in case of a He-probing beam are given for three different scattering angles (5, 7.5 and 10 degrees). It is clear from Fig. 14 that the scattering by

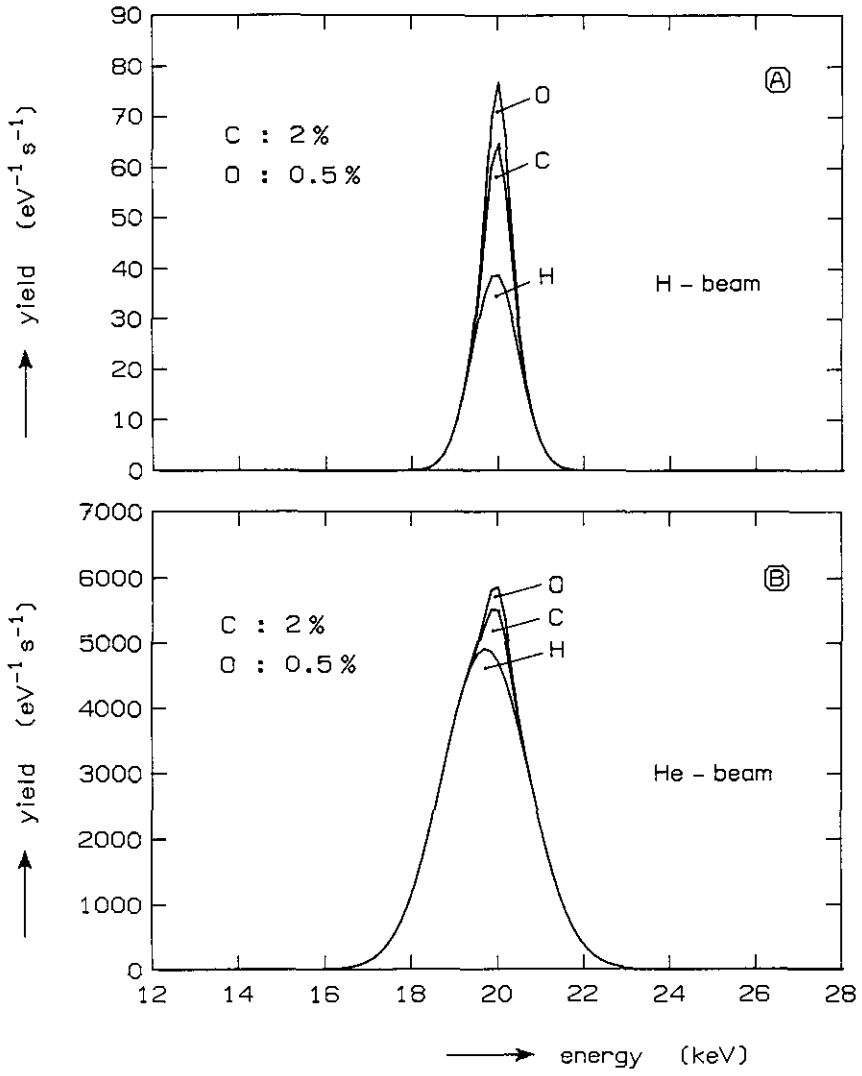

Fig. 13. Scattering distribution for a H-beam (Fig. 12a) and a He-beam (Fig. 12b) in case of an 800 eV hydrogen plasma with 2% C and 0.5% O impurities.

impurities can be more easily discriminated from scattering by protons at larger scattering angles. The price one has to pay for this is a decrease of the total scattering yield, which might be tolerable under most circumstances.

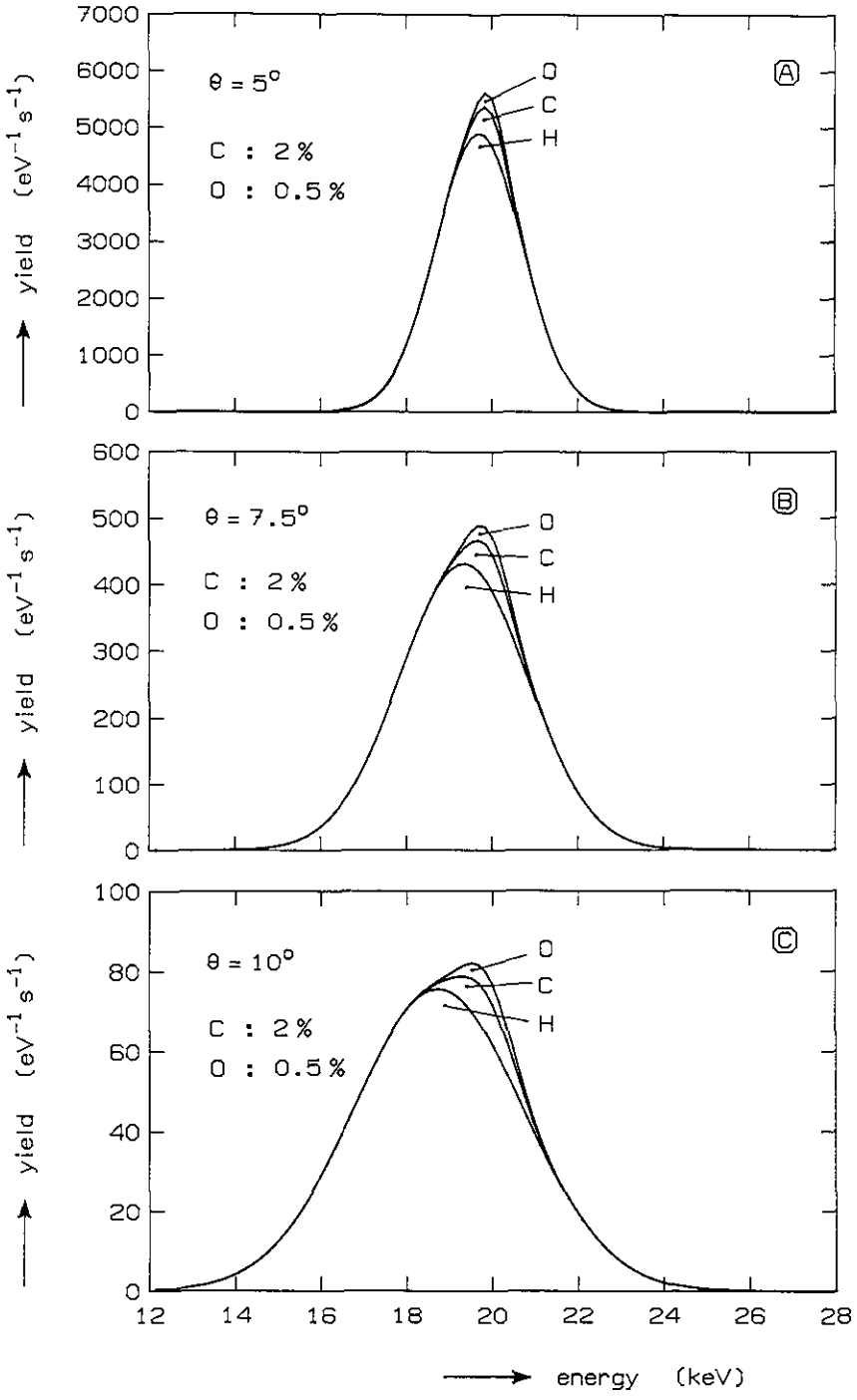

Fig. 14. Scattering distribution for a He-beam in an 800 eV hydrogen plasma polluted with 2% C and 0.5% O for three different scattering angles.

7. HYDROGEN VERSUS HELIUM PROBING BEAMS

The results in the previous sections clearly point to He being the best candidate for the probing particle in a Rutherford-scattering experiment at TEXTOR. There are several reasons why He is a better choice than H. Firstly, the attenuation of a He-probing beam is about a factor 7 smaller than that of a H-beam. Secondly, losses due to resonant charge exchange during the Rutherford-scattering process are one order of magnitude smaller for He than for H. There is also the fact that the thermal broadening of the distribution of scattered neutrals is twice as large for He as for H. The integrated scattering yield when using a He-beam is about a factor 200 larger than when using hydrogen. A consequence of the large thermal width of the He-distributions is the fact that instrumental effects give only rise to a small additional broadening. Finally, it has to be emphasized that the effect of impurities on the total scattering distribution makes it almost impossible to extract information about the proton temperature in case that a H-probing beam is used. When using a He-beam, however, the scattering from impurities is clearly separable from the proton distribution.

From Figs. 4-13, we can give already an estimate for the optimum values for a Rutherford-scattering experiment at TEXTOR, using a He-probing beam. The optimum energy will be in the range $15 < E_b < 25$ keV since in this region both attenuation and resonant charge-exchange losses are at a minimum. The scattering angle must be chosen in the range $5° < \theta < 10°$, slightly dependent on the ion temperature in the plasma. For T = 800 eV the total scattering distribution fits well into the $\pm$ 20% bandwidth of the analyser up to a scattering angle of 10°.

8. THE RUTHERFORD-SCATTERING EXPERIMENT AT TEXTOR

The case of a nearly steady-state ohmically-heated plasma using one particle component (hydrogen or deuterium) with small amounts of impurities present, will be suitable to demonstrate the potentialities of the method which is of practical importance. If deuterium is the main plasma component, however, it is not easy to separate the contributions of the impurities from the total scattering distribution straightforwardly (see Fig. 15a and b corresponding to T = 800 eV and 1600 eV, respectively) as in the case of a proton plasma (see Figs. 14a,b,c). When the amount of the different impurities is known from an independent observation, it will still be possible to deduce the local temperature of deuterium in the core with good accuracy.

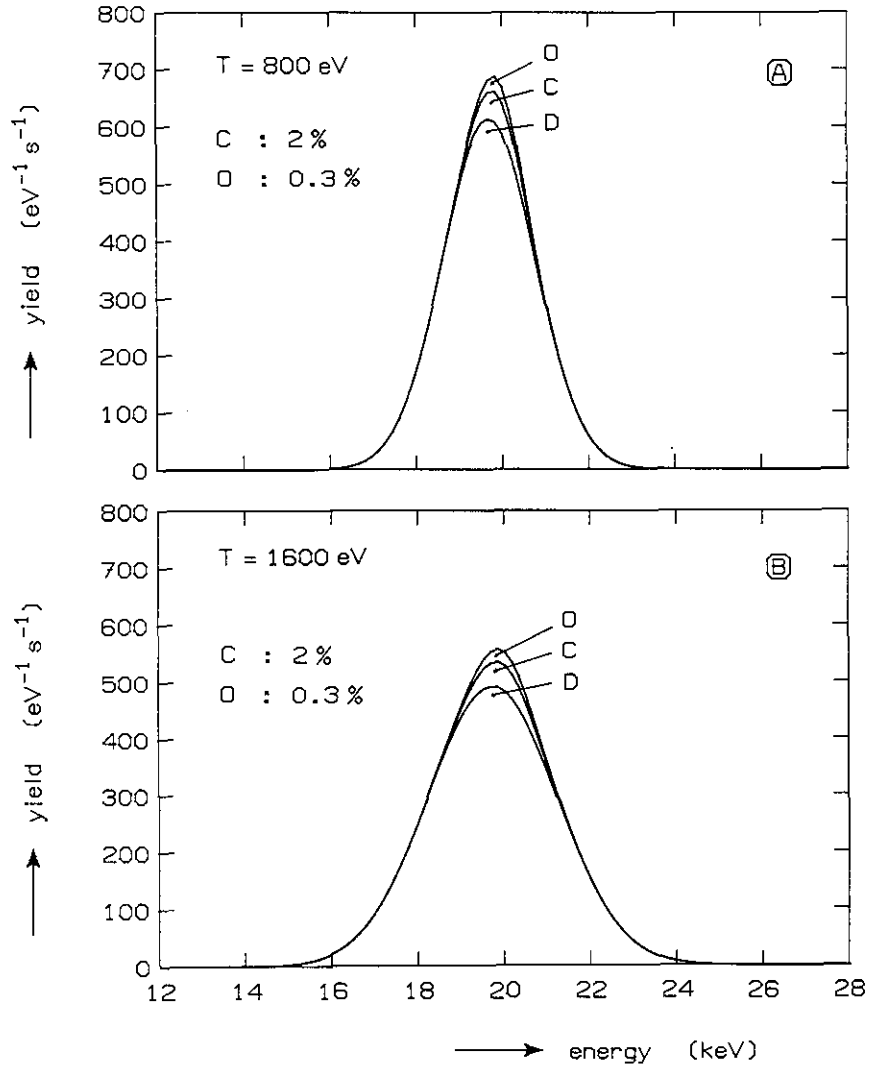

Fig. 15. Scattering distribution for a He-beam in a TEXTOR deuterium plasma (2% C and 0.3% O) for two different temperatures. Scattering angle: 7.5°.

It is also possible to vary the amount of impurities in the experiment and to study the effect of this variation on the total scattering distribution to attain correction factors, which will, anyhow, be small in relation to the measured value. It has to be realized that under ohmically-heating conditions sawtooth-induced effects can be followed with sufficient time resolution, which we state to be at least 3 ms.

Ion-cyclotron heating (ICRH) is employed at TEXTOR to increase the ion temperature of the plasma. In this context, one can consider the observation of the ion-velocity distribution before and during the heating phase to be very desirable, if not necessary. The energy spectrum to be expected in the case of additional heating will deviate from a maxwellian distribution. The ICRH adds another component (H or ^{3}He < 10%) to the plasma by working under minority-heating conditions. Hence, a strong deviation from a maxwellian distribution can be expected for the minority component. This distribution is super-imposed but slightly shifted on the energy scale with respect to the deuterium-scattered spectrum. The possibility to separate both spectra is limited.

In Fig. 16, the effect of 10% of hydrogen on the total distribution is shown in case of thermal equilibrium. The hydrogen contribution is hardly visible. Hence, one only measures the temperature of the deuterium component. If the temperature of the H-minority increases due to the ICRH, its distribution will broaden and will become even more negligible. In the case of ^{3}He the situation is different (see Fig. 17). Here, the two spectra cannot be separated easily. The concentration of ^{3}He, however, can be varied in the experiments within certain limits, and can be used as a free parameter.

In Fig. 18, the effect of a H- and a ^{3}He-minority component on the FWMH of the total distribution is plotted. The temperatures of minority and majority components were taken equal. 10% of H does not influence the FWHM. The width of the distribution is 4% smaller for 10% of ^{3}He than in a pure deuterium plasma. If the amount of ^{3}He is known within a few percent, the correction to be applied to the measured T is smaller than 1%. The dependence of the curves in Fig. 18 on the ion temperature and on the scattering angle is negligibly small.

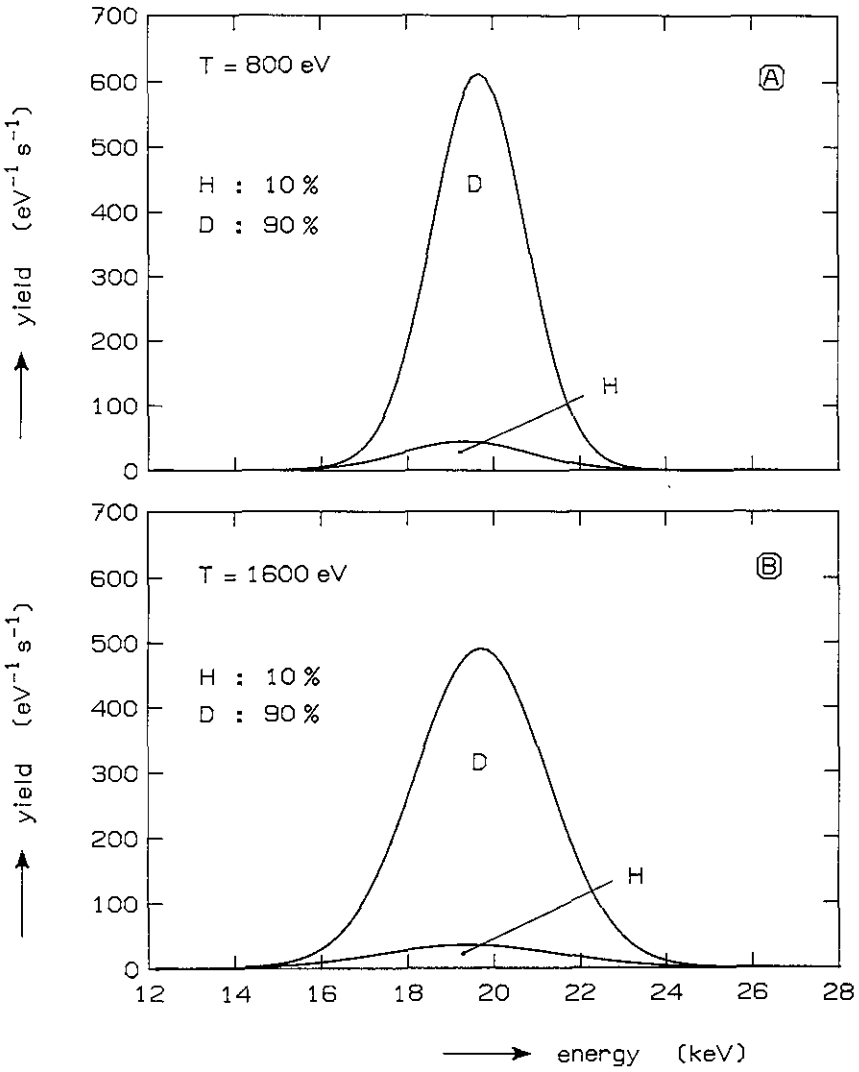

Fig. 16. Scattering distributions of a He-beam in a deuterium plasma with 10% of hydrogen minority for two different temperatures at $\theta = 7.5°$.

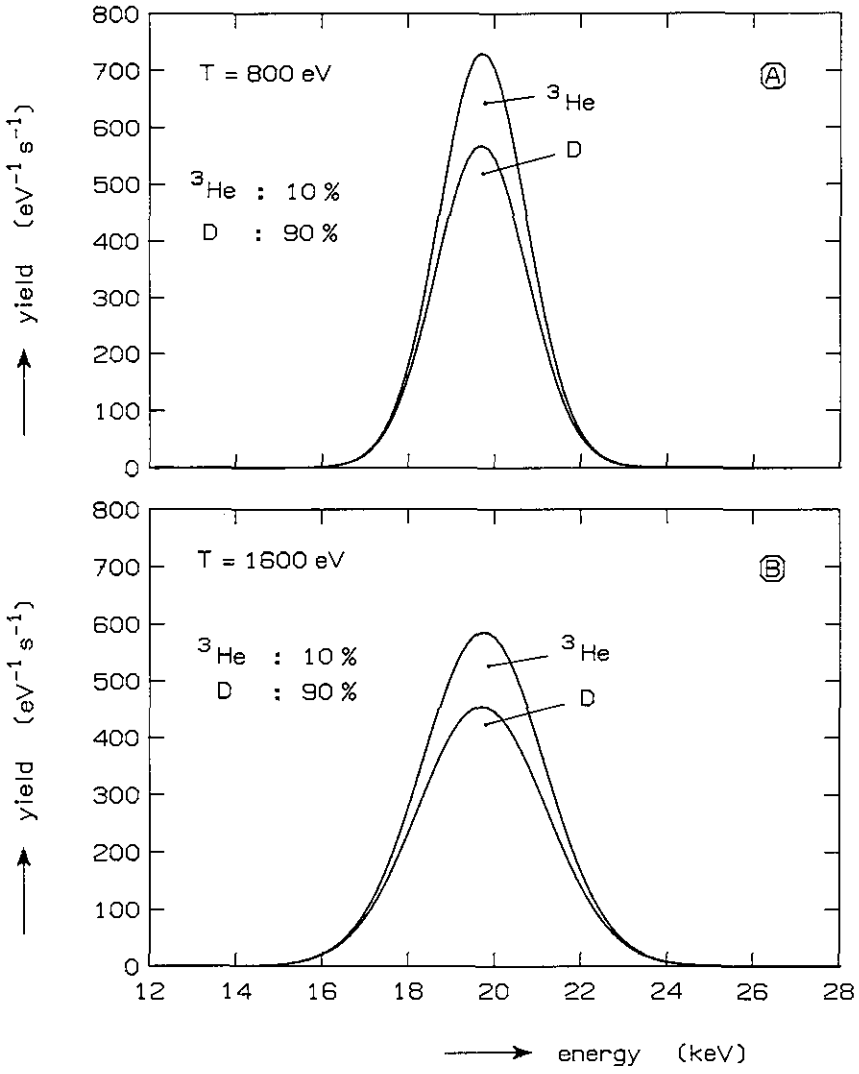

Fig. 17. Scattering distribution of a He-beam in a deuterium plasma with 10% of ^{3}He minority for two different temperatures at $\theta = 7.5^\circ$.

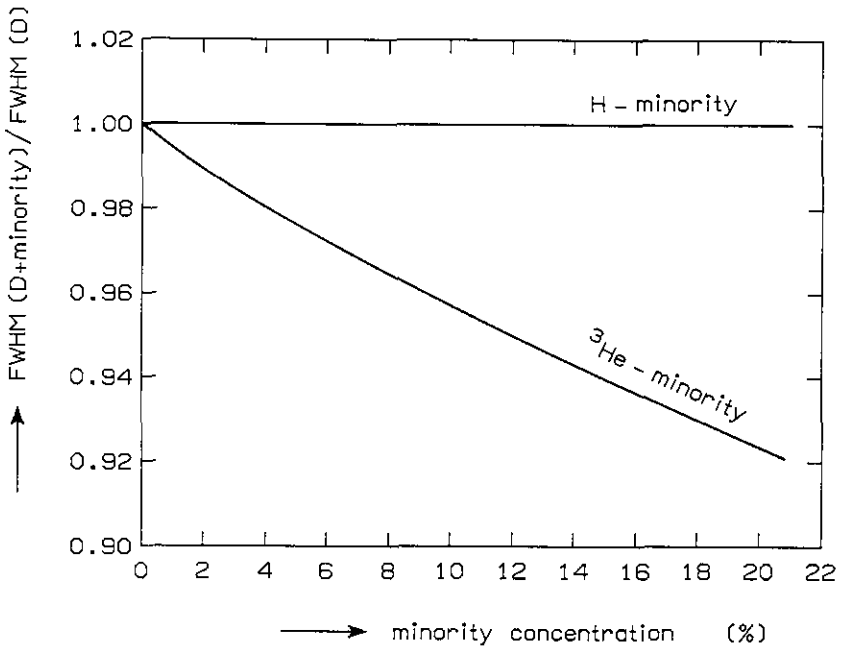

Fig. 18. The influence of different minority concentrations on the FWHM of the total scattering distribution.

If the temperatures of minority and majority components are not equal, the effect on the FWHM of the total distribution becomes different. We express the temperature of the ^{3}He-minority as $T_{^3He} = a \times T_D$, and investigate the effect of the minority on the total FWHM for different values of a. This is done in Fig. 19, ranging the value of a from 1 to 3. A special case occurs if a = 1.5, where the width of the minority component is equal to that of the majority component and no net effect is seen on the total FWHM, irrespective of the minority concentration. If a > 1.5, the effect of 10% ^{3}He-minority results in an increase of the total FWHM.

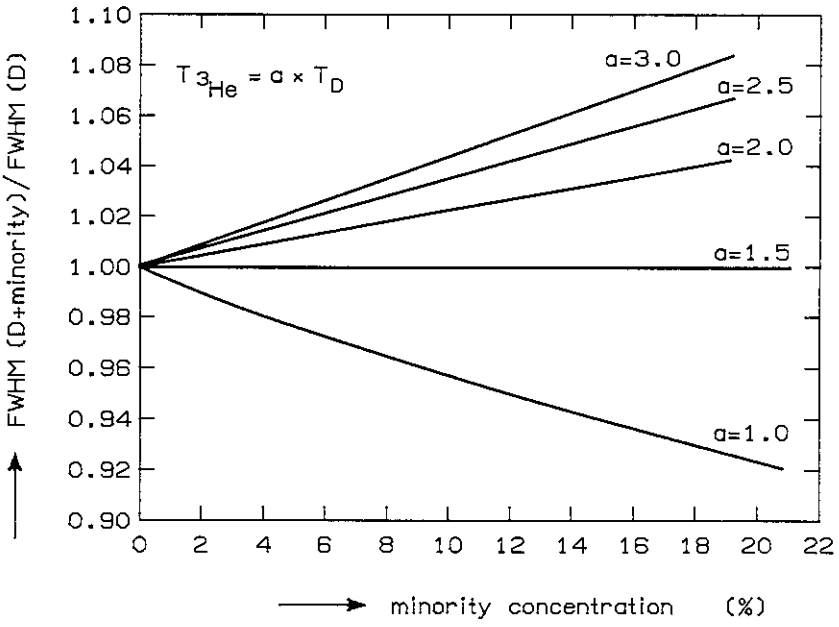

Fig. 19. The influence of different ^{3}He-concentrations on the FWHM of the total scattering distribution for various values of the minority temperature. The deuterium temperature is 800 eV in all cases.

9. SUMMARY

Rutherford scattering of energetic neutrals is a very suitable method to measure the energy distribution of plasma ions with good space and time resolution. Furthermore, the interpretation of the measurements is comparatively straightforward.

The feasibility study is based on the properties of the FOM time-of-flight analyser and the parameters of the TEXTOR tokamak. A 20 keV diagnostic He-beam with a current density of about 10 A/m^2 appears to be a proper choice for the intended experiment. Helium is strongly to be preferred above hydrogen in this parameter field. The time resolution of better than 3 ms will be sufficient to follow events connected with sawtooth phenomena. The spatial resolution will be 0.20 m in the vertical and 0.02 m in the horizontal direction.

The influence of impurity ions is thoroughly investigated and appears to be not disturbing. There are strong indications that upon scattering by heavy impurity ions, the incoming neutral atoms lose with high probability an electron during the scattering process, and the scattering cross-section from these impurities is therefore accordingly reduced. It appears from the computed data that the influence of impurities might be only severe in the case of a hydrogen probing beam in contrast to the preferred He-beam. There is, in principle, an option to separate the contributions from heavy impurities by variation of the observational angle, but reproducible discharge conditions are then required.

The high energy resolution of the time-of-flight analyser allows for the registration of distinct structures appearing on the energy distribution. This is of value especially if a complex situation, as expected during additional plasma heating, has to be analysed. In the case of minority heating with ICRH, the spectrum of Rutherford-scattered neutrals is composed of two components. If a 10% hydrogen population is added to deuterium, the scattering experiment will respond to the majority component only. In the case of a 10% ^{3}He-component, again a disturbing influence on the determination of the temperature of the majority component will remain quite small. In either case the minority component remains shielded and cannot be observed.

The beam will preferentially be placed vertically with respect to the equatorial plane, i.e. perpendicularly to the magnetic field gradient and to neutral-particle heating beams. The good spatial resolution allows for the investigation of the local energy deposition during ion-cyclotron

wave heating and during neutral-beam injection. The Rutherford-scattering diagnostic can contribute to a better understanding of heating processes in large tokamak plasmas.

ACKNOWLEDGEMENTS

The authors like to thank Prof. Dr. H. de Kluiver and Ing. H.W. van der Ven for useful discussions.

This work was performed as part of the research programme of the association agreement of Euratom and the "Stichting voor Fundamenteel Onderzoek der Materie" (FOM) with financial support from the "Nederlandse Organisatie voor Zuiver-Wetenschappelijk Onderzoek" (ZWO) and Euratom.

VIII REFERENCES

[1] S.S. Medley and R. Persing, Rev. Sci. Instrum. 52 (1981) 1463.

[2] D.R. Slaughter, Proc. APS Top. Conf., Boston, 1982.

[3] M. Bitter et al., 6th Int. Symp. on Temperature: Its Measurement and Control in Industry. Washington, 1982. Princeton Report PPPL-1891 (1982).

[4] P. Woskoboinikow et al., Proc. 7th Int. Conf., Marseille, 1983.

[5] H. Park et al., Nucl. Fusion 25 (1985) 1399.

[6] V.G. Abramov et al., Sov. Phys.-Tech. Phys. 16 (1972) 1520.

[7] E.V. Aleksandrov et al., JETP Lett. 29 (1979) 1.

[8] E.L. Berezovskii, A.I. Kislyakov, S. Ya. Petrov and G.V. Roslyakov, Sov. J. Plasma Phys. 6 (1980) 760.

[9] H.J.B.M. Brocken and H.W. van der Ven, IEEE Trans. Plasma Sci. Vol. PS-9, 3 (1981) 92.

[10] G.H.J. Notermans, H.W. van der Ven and H.J.B.M. Brocken, Rijnhuizen Report 82-140 (1982).

[11] G.H.J. Notermans and H.W. van der Ven, Rijnhuizen Report 84-154 (1984).

[12] G.H.J. Notermans, Rijnhuizen Report 84-155 (1984).

[13] G.H.J. Notermans, Rijnhuizen Report 84-157 (1984).

[14] H. Soltwisch et al., Plasma Physics and Controlled Fusion 261A (1984) 23.

[15] A.L. Freeman and E.M. Jones, Culham Report CLM-R 137 (1974).

[16] E.M. Jones, Culham Report CLM-R 135 (1977).

[17] F.P. Ziemba et al., Phys. Rev. A118 (1960) 1552.

[18] G.J. Lockwood and E. Everhart, Phys. Rev. A125 (1962) 567.

[19] H. Takeuchi et al., Jap. J. Appl. Phys. 22 (1983) 1717.

[20] G.H.J. Notermans et al., Nucl. Instrum. Methods 215 (1983) 555.

[21] P. Bogen, IPP Jülich, private communication.